Title

Chapter 6 Block Liposomes Vesicles of Charged Lipids with Distinctly Shaped Nanoscale Sphere-, Pear-, Tube-, or Rod-Segments

Journal

METHODS IN ENZYMOLOGY LIPOSOMES, PT G, 465(C)

ISSN

0076-6879

Authors

Zidovska, Alexandra

Ewert, Kai K

Quispe, Joel

et al.

Publication Date

2009

DOI

10.1016/s0076-6879(09)65006-0

Published in final edited form as:

Methods Enzymol. 2009 ; 465: 111–128. doi:10.1016/S0076-6879(09)65006-0.

Block Liposomes: Vesicles of Charged Lipids with Distinctly Shaped Nanoscale Sphere-, Pear-, Tube-, or Rod-Segments

Alexandra Zidovska[1], **Kai K. Ewert**[1], **Joel Quispe**[2], **Bridget Carragher**[2], **Clinton S. Potter**[2], and **Cyrus R. Safinya**[1,*]

[1]Materials, Physics, and Molecular, Cellular and Developmental Biology Department, University of California at Santa Barbara, Santa Barbara, CA 93106

[2]National Resource for Automated Molecular Microscopy, Department of Cell Biology, The Scripps Research Institute, La Jolla, CA 92037

Abstract

We describe the preparation and characterization of block liposomes, a new class of liquid vesicles, from mixtures of the highly charged (+16 e) multivalent cationic lipid MVLBG2 and 1,2-dioleoyl-*sn*-glycero-3-phosphocholine (DOPC). Block liposomes (BLs) consist of distinct spherical, tubular, and micellar liposomes which remain connected, forming a single liposome. This is in contrast to typical vesicle systems, where distinctly shaped liposomes are macroscopically separated. In a narrow composition range (8-10 mol % MVLBG2), an abundance of micrometer-scale BLs (typically sphere-tube-sphere triblocks) was observed. Cryo-TEM revealed that BLs are also present at the nanometer scale, where the blocks consist of distinctly shaped nanoscale spheres, pears, tubes, or rods. Pear-tube diblock and pear-tube-pear triblock liposomes contain nanotubes with inner lumen diameter 10-50 nm. In addition, sphere-rod diblock liposomes are present, containing rigid micellar nanorods ≈4 nm in diameter and several μm in length. Block liposomes may find a range of applications in chemical and nucleic acid delivery and as building blocks in the design of templates for hierarchical structures.

Introduction

The landmark discovery of liposomes (self-assemblies of lipids) by A. D. Bangham et al. (Bangham *et al.*, 1973) was eventually followed by enormous research efforts in both basic and applied science (Lasic, 1993). Because of their similarities to biological membranes, liposomes are used in model studies of interactions between cells as well as eucaryotic organelles. Liposomes can be used to encapsulate drugs and other chemicals, resulting in important applications in medicine. For example, “stealth” liposomes (Lasic and Martin, 1995) have applications in cancer therapy and cationic liposome-nucleic acid complexes (Huang, 2005) are now used in about 10% of the ongoing human clinical trials for gene delivery (Edelstein *et al.*, 2007; Edelstein *et al.*, 2004).

*Corresponding author: safinya@mrl.ucsb.edu, Tel (805) 893-8635, Fax (805) 893-7221.

In addition to the most common spherical shape of (unilamellar) liposomes, a large variety of vesicle (bilayer-based liposome) shapes has been described, including ellipsoids and oblates, tori, and discocytes and stomatocytes (Chiruvolu *et al.*, 1994; Lipowsky and Sackmann, 1995; Seifert, 1997; Yager and Schoen, 1984). Fig. 1 shows micrographs of complex vesicle morphologies such as a torus (Fig. 1A and B) (Michalet and Bensimon, 1995b), a "button" (Fig. 1C-E) (Michalet and Bensimon, 1995a) and a discocyte (Fig. G-I) (Kas and Sackmann, 1991). In addition, Fig. 2 shows vesicles shaped like tubules (Fig. 2 A) (Chiruvolu *et al.*, 1994), a pear (Fig. 2 B) and a dumbbell (Fig. 2C) (Kas and Sackmann, 1991). Current theoretical treatments, which are consistent with these shapes, include elastic free energy models of membranes described by the membrane bending and Gaussian moduli as well as the spontaneous curvature, at a constant total surface area of the vesicle (Lipowsky and Sackmann, 1995; Safran, 1994).

More recently, substantial research efforts have been directed toward producing lipid-based bio-nanotubes for a range of applications such as storage and controlled release of chemicals and drugs, including nucleic acids, peptides, and proteins (Martin, 1994; Schnur, 1993). The approaches pursued to prepare the nanotubes include the use of templates, e.g., filamentous cytoskeletal proteins such as microtubules, a tubular polymer assembled from dimers of the protein tubulin. In this way, lipid–protein nanotubes with open or closed ends were obtained (Raviv *et al.*, 2005; Raviv *et al.*, 2007). The quest to produce tubular structures solely from lipid components has thus far mainly resulted in the solid phase lipid tubules discovered many years ago (Schnur, 1993). These lipid tubules are typically comprised of unilamellar or multilamellar membranes in their quasi-2D solid phase wrapped around a hollow core, with lengths on the order of several tens of micrometers, and a diameter between ≈100 nm and ≈1 μm (Singh *et al.*, 2003; Spector *et al.*, 2001). Control over the tubule dimensions and properties is important for practical application, and several procedures to generate monodisperse tubules on the micrometer scale have been developed (Shimizu *et al.*, 2005). Custom tailored lipid molecules were synthesized in order to systematically study the impact of the lipid architecture on the tubule formation process. This work identified chirality as one of the prerequisites for forming tubules and helical ribbons from lipid molecules in their chain ordered, quasi-2D solid phase (Spector *et al.*, 2001; Thomas *et al.*, 1995).

While solid-phase lipid tubules can be obtained in systems containing only a single lipid, at least two lipid components are required to generate *liquid* vesicles (consisting of chain-melted lipids) exhibiting the cylindrical tubular structure. One example is a mixture of two lipids, with one exhibiting a cylindrical and the other a conical molecular shape. In this system, a spontaneous breaking of symmetry in lipid composition between the outer and inner layers would generate an initial curvature of the membrane and, in principle, lead to a (energetically favored) cylindrical liquid vesicle structure (Safran, 1994; Safran *et al.*, 1990). Liquid-phase vesicles are of particular high interest because they allow the incorporation of functional biomolecules, which typically require the lipids of the membrane to be in the chain-melted state to retain their full biological activity. Such lipid nanotubes could therefore be useful for a range of applications, including sensing and chemical delivery.

In this chapter, we describe the preparation and characterization of a new, recently discovered class of vesicles, termed block liposomes (BLs) (Zidovska *et al.*, 2009a). BLs

spontaneously form in water from a lipid mixture comprised of the hexadecavalent cationic lipid MVLBG2 and neutral 1,2-dioleoyl-*sn*-glycero-3-phosphatidylcholine (DOPC). They are vesicles consisting of several connected, yet distinctly shaped liposomes such as spheres, pears, tubes and cylindrical micelles (rods). These building units are called blocks in analogy to block copolymers. Fig. 3 schematically depicts a sphere-tube diblock (Fig. 3A), a sphere-tube-sphere triblock (Fig. 3B) and a sphere-rod diblock, containing a cylindrical micelle (Fig. 3C).

Materials and Methods

Liposome Preparation

DOPC was purchased from Avanti Polar Lipids (Alabaster, AL) and dissolved in chloroform. MVLBG2 trifluoroacetate was synthesized as described (Ewert *et al.*, 2006) and dissolved in chloroform/methanol (9:1, v/v). These lipid solutions (at a concentration of 10 or 30 mM, matching the desired concentration of the aqueous solution to be prepared) were combined in glass vials to yield the desired ratio of lipids and dried, first by a stream of nitrogen and subsequently in a vacuum for 8 to 12 hours, to form a thin film on the vial surface. To this film, high resistivity (18.2 MΩ cm, from a Millipore system) water was added and the resulting mixture was incubated at 37 °C for at least 12 hours to give a final concentration of 10 mg/mL (30 mg/mL for micellar solutions). These aqueous lipid solutions were stored at 4 °C until use.

Microscopy

Optical Microscopy was performed using a Nikon Diaphot 300 inverted microscope equipped for epifluorescence and differential-interference-contrast (DIC) and a SensiCam^{QE} High Speed digital camera. For fluorescence microscopy, liposome stock solutions were prepared as described above, but at 1 mmol concentration and with the inclusion of 1 mol % lipid dye Texas Red DHPE (Invitrogen / Molecular Probes).

Cryogenic TEM was used to image the liposome solutions on a nanometer scale. This part of the presented work was conducted at the National Resource for Automated Molecular Microscopy which is supported by the National Institutes of Health through the National Center for Research Resources' P41 program (RR17573). The specimens were preserved in a layer of vitreous ice suspended over a holey carbon substrate. The holey carbon films consist of a thin layer of pure carbon fenestrated by 2 μm holes spaced 4 μm apart and suspended over 400 mesh copper grids, yielding a periodic pattern of holes within a single copper grid segment (Quispe *et al.*, 2007). Carbon coated copper grids were cleaned and activated by oxygen plasma treatment using a Solarus plasma cleaner (Gatan Inc.) and a 25% O_2, 75% Ar mixture. A total of 4 μL of the sample solution was placed on the carbon-coated side of the copper grid. The concentration of the sample solution was varied depending on the structures being imaged. A concentration of 5–10 mg/mL was used for block liposome solutions, while 30 mg/mL was used for micellar lipid solutions. The copper grid with the sample solution was mounted into a Vitrobot (FEI), which blotted the sample for 3, 4 or 5 s, thus varying the sample thickness, and subsequently vitrified the sample by plunge-freezing into a liquid ethane bath. The vitrified sample was then imaged using a

Tecnai F20 electron microscope (FEI Co.) at 120 keV. Images were collected using a 4096 × 4096 pixel CCD camera (TVPIS GmbH) at the search magnification of 5,000× and final magnifications of 29,000× to 280,000× at an underfocus of ~2.5 μm. The Leginon software system (Suloway *et al.*, 2005) was used for data collection, data storage as well as partial data analysis.

Results and Discussion

Design and Synthesis of MVLBG2

The highly charged, cone-shaped lipid MVLBG2 is based on a previously described lipid building block with two oleyl chains (Schulze *et al.*, 1999). The oleyl chains were selected since they will form liquid-phase membranes at room temperature and ensure compatibility with DOPC membranes. The synthesis of the headgroup was designed in a way to allow the introduction of a high number of charges with a small number of chemical steps. To this end, ornithine was employed as a dendritic AB_2 building block. In combination with a previously prepared, Boc-protected building block for a tetravalent headgroup (Behr, 1989), this allowed assembly of the headgroup using efficient peptide-coupling and –deprotection methods. The resulting, gram-scale synthesis of MVLBG2 has been described in a previous paper (Ewert *et al.*, 2006). Fig. 4A shows the chemical structure of MVLBG2 which has a headgroup charge of +16 e at full protonation. The hydrophobic tail, spacer, ornithine branching units and charged carboxyspermine moieties are underlaid in tan, blue, green and red, respectively. The pH of the aqueous lipid solutions used in our experiments was measured using indicator paper (due to the small sample volume) as 5.5 ± 0.5, which corresponds to an average MVLBG2 charge of +14.5 e to +16 e.

Phase Behavior of MVLBG2/DOPC Lipid Mixtures

While the extreme mismatch in headgroup area versus tail area of MVLBG2 results in a conical molecular shape, the charge-neutral zwitterionic 1,2-dioleoyl-*sn*-glycero-3-phosphatidylcholine (DOPC) has a cylindrical molecular shape with its headgroup area nearly equal to its tail area. Space filling molecular models of MVLBG2 and DOPC illustrating the different molecular shapes of the two lipids are shown in Fig. 4B. Both lipids are in their chain-melted state at room temperature due to the presence of a *cis* double bond in their oleoyl chains. Given this combination of molecular properties, MVLBG2/DOPC mixtures in water appeared to be a promising system for the formation of cylindrical liquid vesicles. Indeed, wide-angle X-ray scattering experiments confirmed that the lipids remained in their chain-melted liquid state in all investigated samples (data not shown).

The phase behavior of the MVLBG2/DOPC/water system is extremely rich. We initially used DIC microscopy to investigate the liposome structures formed on a micrometer scale (Zidovska *et al.*, 2009a). Fig. 5 A through G displays DIC microscopy images of vesicles undergoing shape transitions as a function of their lipid composition. Membranes with very high DOPC content exhibit predominantly polydisperse multilamellar onion-like vesicles for 0–8 mol % MVLBG2 (Fig. 5A). Unexpectedly, a phase consisting of a nearly uniform block liposome population was found in a very narrow composition interval of ≈8–10 mol % MVLBG2 (Fig. 5B). Its hallmark is the ≈5 μm long cylindrical core of diameter ≈0.5 μm,

capped with quasi-spherical vesicles a few μm in diameter at both ends (Fig. 5C). With increasing MVLBG2 content in the sample, the system first reenters a regime of polydisperse, multilamellar onion-like vesicles (Fig. 5D). Then, at ≈25 mol % MVLBG2, the polydisperse vesicles are replaced by a fairly monodisperse population of spherical vesicles of diameter ≈2 μm (Fig. 5E). As the MVLBG2 content increases further, a regime of coexistence between micelles and vesicles is reached around 50 mol % MVLBG2 (Fig. 5F). In DIC microscopy, this sample appears sparsely populated with only occasional vesicles. The vesicle aggregation observed in this region results from depletion attraction forces, mediated by the micelles. At MVLBG2 contents above 75 mol %, vesicles disappear and only micelles are present. Since the size of the micelles is below the optical resolution of DIC microscopy (Fig. 5G), we employed fluorescence imaging to prove their existence (Fig. 5H), and cryo-TEM to determine their size and morphology (Fig. 5I). As shown in Fig. 5I, cryo-TEM shows that samples containing 75 mol % MVLBG2 consist of a dense solution of disc-shaped micelles ≈4 nm thin and of ≈10 nm diameter. The micelle morphology changes with MVLBG2 content, and at 100 mol % MVLBG2, monodisperse spherical micelles of diameter ≈4 nm populate the sample (Zidovska et al., 2009b).

Block Liposomes

As mentioned above, DIC microscopy revealed an evolution in vesicle shape on the micrometer scale from spherical vesicles to block liposomes (BLs) in a narrow composition range (8–10 mol % MVLBG2). BLs constitute a remarkable new class of vesicles. Most importantly, BLs are unique in that well known distinct liposome morphologies such as spheres, tubules or cylindrical micelles, appear as connected parts within a single BL. This provided the rational for naming these new structures, in analogy to block copolymers. As in the morphologies of block copolymers, BLs exhibit a microphase separation of well defined shapes within a single BL, as opposed to macrophase separation, where these shapes would not be connected.

Furthermore, the Gaussian membrane curvature distinguishes BLs from previously described vesicle morphologies. Fig. 6 shows a schematic comparison of a block liposome and a dumbbell vesicle. This illustration visualizes membrane regions distinct Gaussian curvature using different colors. Membrane regions exhibiting positive Gaussian curvature are depicted in red, negative Gaussian curvature is shown in blue and zero Gaussian curvature in yellow. The schematic demonstrates that a block liposome consists of membrane regions of three different Gaussian curvatures: positive, zero and negative, unlike the dumbbell morphology which can be described by only two distinct Gaussian curvatures: positive and negative. Of note, the previously observed pear and dumbbell morphologies are intermediate stages in the proposed mechanisms of block liposome formation (Zidovska, 2009a).

Nanoscale Studies of Block Liposomes

The novel BL morphology persists from the micrometer scale (as shown by DIC microscopy) down to the nanometer scale (Zidovska et al., 2009a). Cryo-TEM (Fig. 7) revealed diblock (sphere–tube) liposomes and triblock (sphere–tube–sphere) liposomes containing nanometer scale tubules of diameter 10–50 nm and length >1μm. These

nanoscale block liposomes are the first examples of synthetic lipid systems forming tubular vesicles in the chain-melted liquid phase while exhibiting an inner lumen of truly nanometer-scale dimensions.

The series of cryo-TEM images shown in Fig. 7 reveal the detailed features of typical di- and triblock liposomes with tubular sections. Two triblock (pear–tube–pear) liposomes (with vesicles of asymmetric size capping the tube) can be seen in Fig. 7A. The high-magnification inset proves that the tubular section has an inner lumen diameter of ≈10 nm (Fig. 7B). A diblock (pear–tube) liposome with inner diameter of ≈50 nm is seen in Fig 7C. We frequently observe one block liposome encapsulated within another block liposome (Fig. 7D and 7E (top arrow)). In these cases, the inner, smaller diameter tubule is observed to protrude through the encapsulating membrane, demonstrating its high bending rigidity. This high bending rigidity and the extraordinarily large persistence length of the order of mm are likely a result of the high charge density of the membrane. Fig. 7E also shows a diblock liposome (lower arrow) and parts of several block liposomes (second, third, and fourth arrows from bottom), which are either di- or triblocks. Schematics of these typical block liposomes containing tubular sections are shown in Fig. 7F (molecular-scale enlargements exposing the inside shown in (a) and (b)). The length of the nanotubule sections evident in these images ranges from around 500 nm to >1 μm.

In addition to BLs with tubular sections, another type of block liposomes is found, which contains highly rigid lipid nanorod sections comprised of cylindrical micelles. A spontaneous topological transition from tubes (cylindrical vesicles) to rods (cylindrical micelles) leads to the formation of this population of sphere–rod diblock liposomes (Zidovska *et al.* 2009a). Fig. 8 (A–D) shows typical images of these remarkable diblock liposomes which demonstrate that the micellar nanorods remain attached to the spherical vesicles. The nanorod diameter equals the thickness of a lipid bilayer (≈4 nm), corresponding to the hydrophobic core of the rod which exhibits high contrast in cryo-TEM. The nanorods can reach up to several μm in length, corresponding to an aspect ratio of the order of 1000, and are very stiff, again exhibiting persistence lengths on the millimeter scale. A lower magnification image (Fig. 8 D) shows a collection of these sphere–rod BLs with a variety of spherical vesicle sizes. Schematics of this novel block liposome structure based on the hypothesized mechanism of their formation are shown in Fig. 8 E. The region where the lipid nanorod is connected to the spherical bilayer vesicle is a true mathematical singularity, analogous to the core of a liquid crystal (−1/2) disclination (de Gennes and Prost, 1993). The high rigidity of the nanorods observed in cryo-EM is consistent with the Odijik–Skolnick–Fixman (OSF) theory of polyelectrolytes (Odijk, 1977; Skolnick and Fixman, 1977), where for $b < L_B$, the electrostatic persistence length $\xi_p = \lambda_D^2/4L_B \approx 300$ μm. Here, b is the distance between charges ≈2 Å for MVLBG2, $L_B = 7.1$ Å the Bjerrum length in water, and $\lambda_D \approx 1$ μm the Debye length in deionized water.

Fig. 9 (A and B) plots the results of a statistical analysis of the nanotube and nanorod populations, including the diameter distribution within the tube population. The diameter histograms weighted by the surface area—indicative of the amount of lipid in the nanorod and nanotube state—and by the length of the structure—highlighting the striking length of nanorods compared to nanotubes—are shown in Fig. 9 A and 9 B, respectively.

The evolution of shapes in the block liposome regime, from spherical vesicles to the block liposomes, is reminiscent of shape changes in biological cellular systems. The striking resemblance to the evolving shape of the plasma membrane of a cell during cytokinesis suggests that membrane-associated molecules (e.g. membrane proteins or glycophospholipids) with physical properties similar to MVLBG2 may aid the out-of-equilibrium (motor driven) process of tubule formation, during late stage cytokinesis just before fission and the splitting of the daughter cells (Reichl *et al.*, 2005; Robinson and Spudich, 2004). Similarly, the triblock liposome state with a narrow tubule connecting quasi-spherical vesicles has a striking resemblance (in shape and size) to bacterial conjugation where a tubular section connects neighboring bacteria exchanging genetic material (Brock, 1994).

We have previously proposed possible mechanisms for the formation of BLs. Importantly, our data excludes the possibilty that nanoscale BLs are formed as a sample preparation artifact, e.g. by flow effects. While the tube and rod segments seem to align to some extent – flow orientation is expected for structures with aspect ratios as high as the BLs confined in a thin layer of water (~ 200 nm) – their orientation is not as uniform as one would expect if they were *generated* by flow. Furthermore, Fig. 10 A shows a rare example of a vesicle membrane shape evolving from a sphere to a sphere with four protruding symmetrical processes, resembling a clover leaf with four leaflets (instead of the more typical single process leading to the diblock (pear–tube) liposome). Such a structure could not be generated by blotting-induced flow.

Further evidence that electrostatic forces resulting from the conically shaped, charged lipid MVLBG2 are the driving force for the creation of BLs is provided by imaging of the BL-forming lipid mixture at high salt conditions (250 mM NaCl, Debye length ≈0.6 nm, effectively screening the electrostatic forces). Block liposomes are not stable under these conditions and are replaced by multilamellar vesicles with spherical topology (Fig. 10 B), independent of whether salt is added to BLs or whether the lipid mixture is hydrated with the salt solution.

While sensitive to salt, BLs are long-lived structures in water and may be dehydrated and reversibly rehydrated. When dried, the spherical caps at the end of the cylindrical core collapse (Fig. 11A). After rehydration, block liposome resume their original shape (Fig. 11B). This capacity might be of use for potential drug storage and/or drug delivery applications. DIC microscopy performed at regular intervals over the course of more than a year experiments revealed no change in morphology, proving that the μm-scale multilamellar block liposomes are long-lived. Similarly, the time intervals between BL preparation and vitrification for cryo-TEM varied, reaching up to two months without showing an effect on the observed structures (Zidovska *et al.*, 2009a). Another piece of evidence suggesting that BLs are not only robust, long-lived structures but equilibrium structures is the fact that in all 426 EM images analyzed, not a single instance of macrophase separation of elongated vesicle shapes, i.e. an isolated tubular vesicle or cylindrical micelle which is not part of a BL, was observed. Spherical structures were the only liposomes observed in the samples alongside the BLs. While our observations suggest that BLs are equilibrium structures, we cannot rule out the possibility that they are kinetically trapped structures with barriers much

larger than the thermal energy. Further investigations, e.g. preparation of liposome solutions by methods other than simple film hydration may clarify this point.

Conclusions

The discovery of block liposomes demonstrates that the addition of a single type of lipid molecule with highly conical shape – imparted to a large extent by electrostatics – to neutral vesicles can lead to a dramatic membrane shape evolution leading to long-lived robust structures. Another recent report also described the formation of tubules upon addition of ganglioside lipids with large headgroups to DOPC-containing vesicles in the presence of salt (Akiyoshi *et al.*, 2003). These membrane shape evolutions have analogies in nature and in the flow of certain abstract geometric shapes in topology which follows the "Ricci flow equation" used to describe surfaces where regions of high curvature diffuse into lower curvature regions (e.g. to generate the flow of shapes from a sphere (positive curvature) to a dumbbell-shaped surface containing negative curvature regions) (Collins, 2004; Mackenzie, 2006). The nanotubes and nanorods may become desirable candidates for drug/gene delivery applications (Ewert *et al.*, 2005; Huang, 2005; Raviv *et al.*, 2005; Raviv *et al.*, 2007; Schnur, 1993; Shimizu *et al.*, 2005; Singh *et al.*, 2003; Thomas *et al.*, 1995) or as template for nanostructures such as wires or needles. Future studies involving systematic variations in the shape, size and charge of the curvature-stabilizing lipid will be aimed at controlling the tubule diameter distribution. Of note, current state-of-the-art analytical theories (Seifert, 1997) and simulations of membrane shapes (Reynwar *et al.*, 2007), which incorporate coupling between curvature and composition, are not able to predict our experimentally discovered block liposomes which are comprised of distinctly shaped but connected liposomes. This may be due to the omission of electrostatic forces in current theories and simulations, which are key to the formation of block liposomes as described above. New theories of charged membranes are required to describe block liposomes. Finally, it seems possible to produce analogous block polymersomes in mixtures of charged and neutral co-polymers (Discher *et al.*, 1999) or peptides (Deming, 1997).

Acknowledgments

This work was supported by DOE grant DE-FG02-06ER46314, NSF grant DMR-0803103, and NIH grant GM-59288. Some of this research was conducted at the National Resource for Automated Molecular Microscopy, which is supported by the NIH National Center for Research Resources P41 program (RR17573).

References

Akiyoshi K, Itaya A, Nomura SM, Ono N, Yoshikawa K. Induction of neuron-like tubes and liposome networks by cooperative effect of gangliosides and phospholipids. FEBS Lett. 2003; 534:33–38. [PubMed: 12527358]

Bangham AD, Hill MW, Miller NGA. Preparation and Use of Liposomes as Models of Biological membranes. Methods Membr. Biol. 1973; 1:1–68.

Behr JP. Photohydrolysis of DNA by Polyaminobenzenediazonium Salts. J. Chem. Soc.-Chem. Commun. 1989:101–103.

Brock, TD.; Madigan, MT.; Martinko, JM.; Parker, J. Biology of Microorganisms. Prentice Hall, New Jersey: 1994.

Chiruvolu S, Warriner HE, Naranjo E, Idziak SHJ, Raedler JO, Plano RJ, Zasadzinski JA, Safinya CR. A Phase of Liposomes with Entagled Tubular Vesicles. Science. 1994; 266:1222–1225. [PubMed: 7973704]

Collins GP. The shapes of space. Sci. Am. 2004; 291:94–103. [PubMed: 15255593]

de Gennes, PG.; Prost, J. The Physics of Liquid Crystals. Oxford University Press; 1993.

Deming TJ. Facile synthesis of block copolypeptides of defined architecture. Nature. 1997; 390:386–389. [PubMed: 9389476]

Discher BM, Won YY, Ege DS, Lee JCM, Bates FS, Discher DE, Hammer DA. Polymersomes: Tough vesicles made from diblock copolymers. Science. 1999; 284:1143–1146. [PubMed: 10325219]

Edelstein ML, Abedi MR, Wixon J. Gene therapy clinical trials worldwide to 2007 - an update. J. Gen. Med. 2007; 9:833–842.

Edelstein ML, Abedi MR, Wixon J, Edelstein RM. Gene therapy clinical trials worldwide 1989-2004 - an overview. J. Gen. Med. 2004; 6:597–602.

Ewert KK, Ahmad A, Evans HM, Safinya CR. Cationic lipid-DNA complexes for non-viral gene therapy: relating supramolecular structures to cellular pathways. Expert Opin. Biol. Ther. 2005; 5:33–53. [PubMed: 15709908]

Ewert KK, Evans HM, Zidovska A, Bouxsein NF, Ahmad A, Safinya CR. A columnar phase of dendritic lipid-based cationic liposome-DNA complexes for gene delivery: Hexagonally ordered cylindrical micelles embedded in a DNA honeycomb lattice. J. Am. Chem. Soc. 2006; 128:3998–4006. [PubMed: 16551108]

Huang, L.; Hung, M-C.; Wagner, E. Non-Viral Vectors for Gene Therapy. Elsevier; San Diego: 2005.

Kas J, Sackmann E. Shape Transitions and Shape Stability of Giant Phospholipid-Vesicles in Pure Water Induced by Area-to-Volume Changes. Biophys. J. 1991; 60:825–844. [PubMed: 1742455]

Lasic, DD. Liposomes: From Physics to Applications. Elsevier; Amsterdam: 1993.

Lasic, DD.; Martin, FJ. Stealth Liposomes. CRC Press; Boca Raton, FL: 1995.

Lipowsky, R.; Sackmann, E. Elsevier; Amsterdam: 1995.

Mackenzie D. Breakthrough of the year - The Poincare conjecture - Proved. Science. 2006; 314:1848–1849. [PubMed: 17185565]

Martin CR. Nanomaterials - a Membrane-Based Synthetic Approach. Science. 1994; 266:1961–1966. [PubMed: 17836514]

Michalet X, Bensimon D. Observation of Stable Shapes and Conformal Diffusion in Genus-2 Vesicles. Science. 1995a; 269:666–668. [PubMed: 17758809]

Michalet X, Bensimon D. Vesicles of Toroidal Topology - Observed Morphology and Shape Transformations. J. Phys. II. 1995b; 5:263–287.

Odijk T. Polyelectrolytes near Rod Limit. J. Polym. Sci., Part B: Polym. Phys. 1977; 15:477–483.

Quispe J, Damiano J, Mick SE, Nackashi DP, Fellmann D, Ajero TG, Carragher B, Potter CS. An improved holey carbon film for cryo-electron microscopy. Microsc. Microanal. 2007; 13:365–371. [PubMed: 17900388]

Raviv U, Needleman DJ, Li YL, Miller HP, Wilson L, Safinya CR. Cationic liposome-microtubule complexes: Pathways to the formation of two-state lipid-protein nanotubes with open or closed ends. Proc. Natl. Acad. Sci. U.S.A. 2005; 102:11167–11172. [PubMed: 16055561]

Raviv U, Nguyen T, Ghafouri R, Needleman DJ, Li YL, Miller HP, Wilson L, Bruinsma RF, Safinya CR. Microtubule protofilament number is modulated in a stepwise fashion by the charge density of an enveloping layer. Biophys. J. 2007; 92:278–287. [PubMed: 17028134]

Reichl EM, Effler JC, Robinson DN. The stress and strain of cytokinesis. Trends in Cell Biology. 2005; 15:200–206. [PubMed: 15817376]

Reynwar BJ, Illya G, Harmandaris VA, Muller MM, Kremer K, Deserno M. Aggregation and vesiculation of membrane proteins by curvature-mediated interactions. Nature. 2007; 447:461–464. [PubMed: 17522680]

Robinson DN, Spudich JA. Mechanics and regulation of cytokinesis. Current Opinion in Cell Biology. 2004; 16:182–188. [PubMed: 15196562]

Safran, SA. Statistical Thermodynamics of Surfaces, Interfaces, and Membranes. Westview Press; 1994.

Safran SA, Pincus P, Andelman D. Theory of Spontaneous Vesicle Formation in Surfactant Mixtures. Science. 1990; 248:354–356. [PubMed: 17784490]

Schnur JM. Lipid Tubules - a Paradigm for Molecularly Engineered Structures. Science. 1993; 262:1669–1676. [PubMed: 17781785]

Schulze U, Schmidt HW, Safinya CR. Synthesis of novel cationic poly(ethylene glycol) containing lipids. Bioconjugate Chem. 1999; 10:548–552.

Seifert U. Configurations of fluid membranes and vesicles. Advances in Physics. 1997; 46:13–137.

Shimizu T, Masuda M, Minamikawa H. Supramolecular nanotube architectures based on amphiphilic molecules. Chem. Rev. 2005; 105:1401–1443. [PubMed: 15826016]

Singh A, Wong EM, Schnur JM. Toward the rational control of nanoscale structures using chiral self-assembly: Diacetylenic phosphocholines. Langmuir. 2003; 19:1888–1898.

Skolnick J, Fixman M. Electrostatic Persistence Length of a Wormlike Polyelectrolyte. Macromolecules. 1977; 10:944–948.

Spector MS, Singh A, Messersmith PB, Schnur JM. Chiral self-assembly of nanotubules and ribbons from phospholipid mixtures. Nano Letters. 2001; 1:375–378.

Suloway C, Pulokas J, Fellmann D, Cheng A, Guerra F, Quispe J, Stagg S, Potter CS, Carragher B. Automated molecular microscopy: The new Leginon system. J. Struct. Biol. 2005; 151:41–60. [PubMed: 15890530]

Thomas BN, Safinya CR, Plano RJ, Clark NA. Lipid Tubule Self-Assembly - Length Dependence on Cooling Rate through a First-Order Phase-Transition. Science. 1995; 267:1635–1638. [PubMed: 17808182]

Yager P, Schoen PE. Formation of Tubules by a Polymerizable Surfactant. Mol. Cryst. Liq. Cryst. 1984; 106:371–381.

Zidovska A, Ewert KK, Quispe J, Carragher B, Potter CS, Safinya CR. Block Liposomes from Curvature-Stabilizing Lipids: Connected Nanotubes, -rods and -spheres. Langmuir. 2009a; 25:2979–2985. [PubMed: 18834165]

Zidovska A, Evans HM, Ewert KK, Quispe J, Carragher B, Potter CS, Safinya CR. Liquid Crystalline Phases of Dendritic Lipid–DNA Self-Assemblies: Lamellar, Hexagonal and DNA Bundles. J. Phys. Chem. B. 2009b; 113:3694–3703. [PubMed: 19673065]

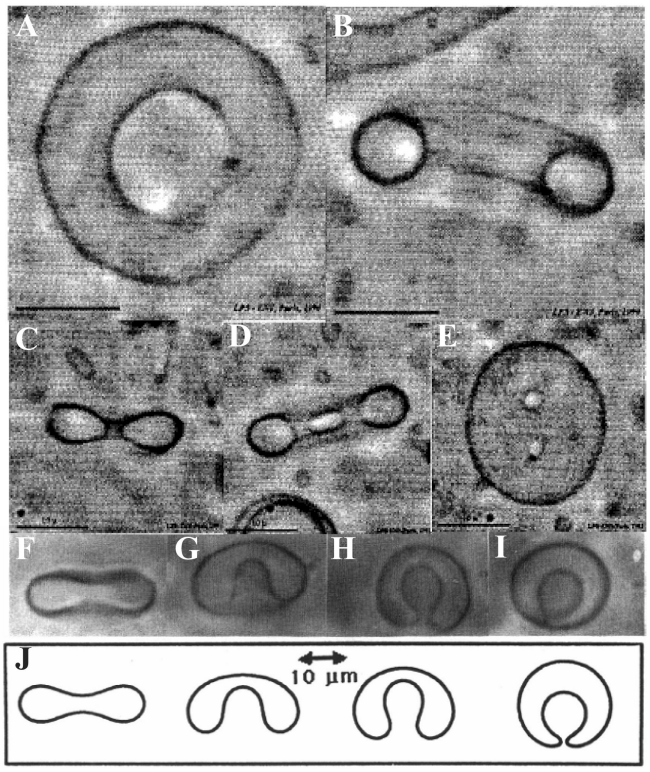

Figure 1. Torus, "button" and discocyte shaped vesicles

A-B, micrographs of a torus vesicle shown from different angles. Reprinted in part from (Michalet and Bensimon, 1995b) with permission. Copyright 1995 EDP Sciences. **C-E,** different views of a button-shaped vesicle. Reprinted in part from (Michalet and Bensimon, 1995a) with permission. Copyright 1995 American Association for the Advancement of Science. **F-J,** different views of a discocyte vesicle (**F-I**) with corresponding schematics (**J).** Reprinted in part from (Kas and Sackmann, 1991) with permission. © 1991 Biophysical Society.

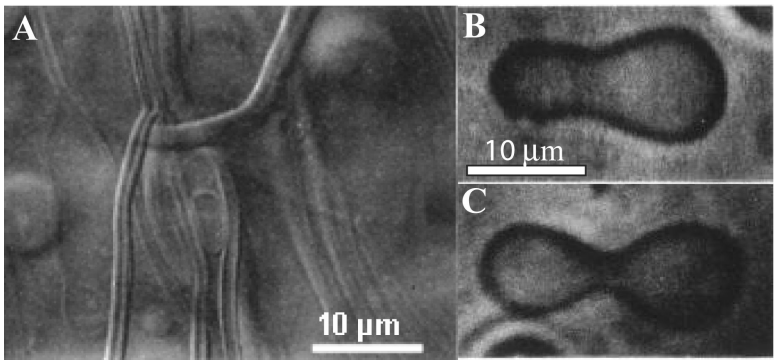

Figure 2. Lipid tubules, pears and dumbbells

A, a micrograph of micrometer scale lipid tubules. Reprinted in part from (Chiruvolu *et al.*, 1994) with permission. Copyright 1994 American Association for the Advancement of Science. **B-C**, images of a pear-shaped (**B)** and a dumbbell-shaped (**C**) lipid vesicle Reprinted in part from (Kas and Sackmann, 1991) with permission. © 1991 Biophysical Society.

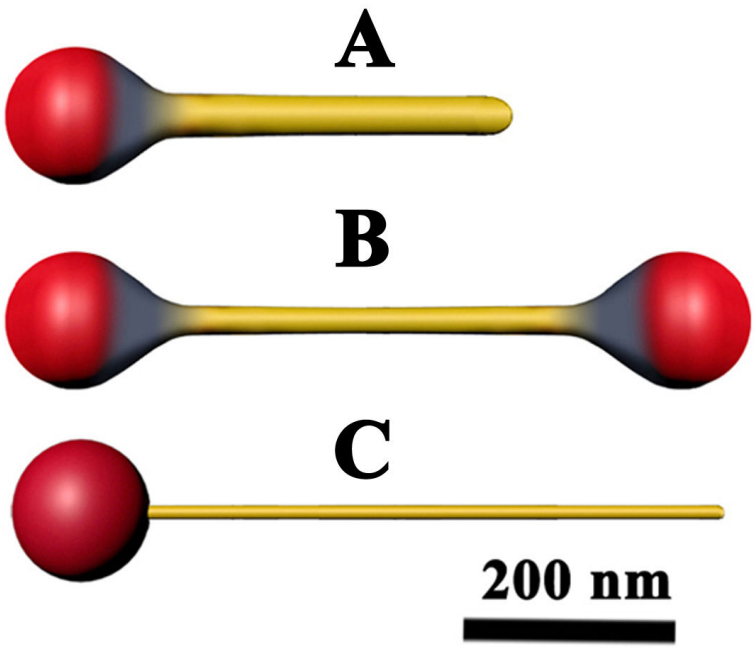

Figure 3. Schematic depiction of the three main types of block liposomes

Different colors coding represent different membrane Gaussian curvature: positive (red), negative (blue) and zero (yellow). **A**, pear–tube diblock liposome. **B**, pear–tube–pear triblock liposome. **C**, sphere–rod diblock liposome. Reprinted in part from (Zidovska *et al.*, 2009a) with permission. Copyright 2008 American Chemical Society.

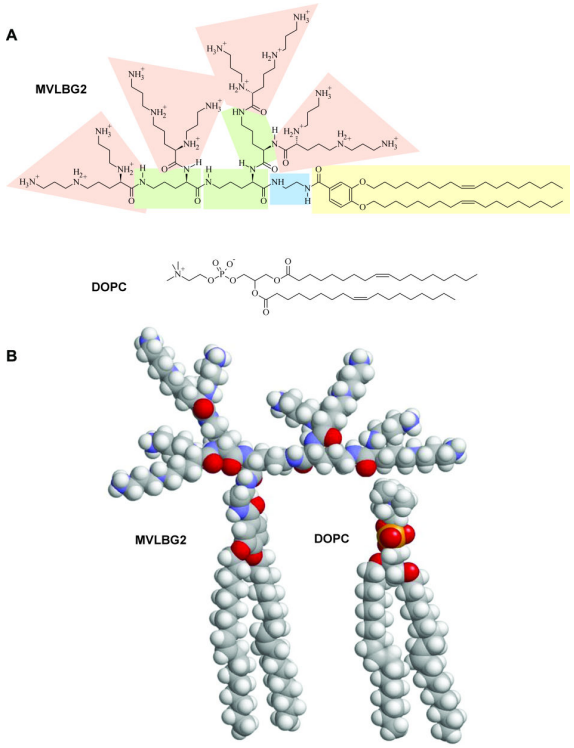

Figure 4. Chemical structures and molecular models of MVLBG2 and DOPC

A, the chemical structures of MVLBG2 and DOPC. **B**, space filling molecular models of MVLBG2 and DOPC demonstrating their conical and cylindrical molecular shape, respectively. Reprinted in part from (Zidovska *et al.*, 2009a) with permission. Copyright 2008 American Chemical Society.

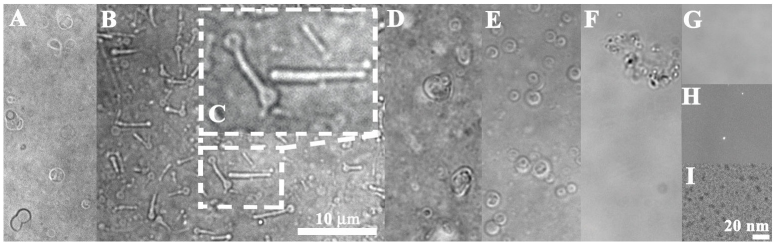

Figure 5. Phase behaviour of the MVLBG2/DOPC/water system

A–G, DIC images of vesicle shapes as a function of their composition: multilamellar spherical vesicles (onions) (0-8 mol % MVLBG2, **A**), block liposomes (8-10 mol % MVLBG2, **B**), reentrant onions (11-50 mol % MVLBG2, **D, E**), macroscopic coexistence of vesicles and micelles (≈50 mol % MVLBG2**, F**) and micelles (75-100 mol % MVLBG2, **G**). **H**, fluorescence microscopy image, demonstrating the existence of micelles. **I**, cryo-TEM image, showing micelle size and morphology. **C**, an inset of (**B**), showing the block liposome morphology in detail: long (≈5 μm) cylindrical cores of diameter ≈0.5 μm capped at both ends with spherical vesicles of a few μm diameter. Reprinted in part from (Zidovska *et al.*, 2009a) with permission. Copyright 2008 American Chemical Society.

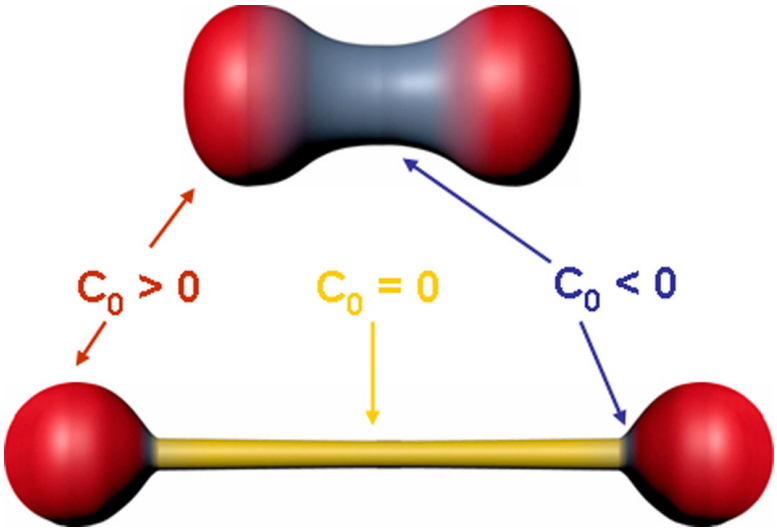

Figure 6. Comparison of the Gaussian curvature of a dumbbell vesicle and a triblock liposome

In the schematic, membrane regions of positive, negative and zero Gaussian curvature are shown in red, blue and yellow, respectively. The illustration demonstrates that regions of all three Gaussian curatures are present in the block liposome, while the dumbbell morphology only contains regions of positive and negative Gaussian curvature.

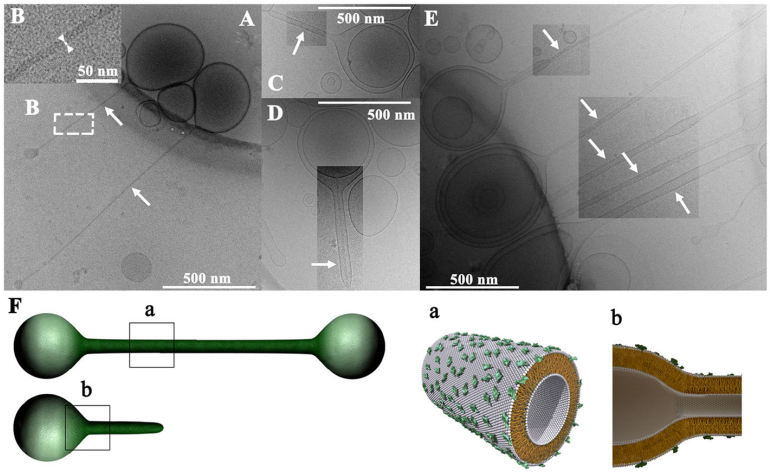

Figure 7. Cryo-TEM images of block liposomes containing liquid-phase lipid nanotubes

A, pear–tube–pear triblock liposomes. **B,** an inset of **A** revealing the hollow tubular structure (white arrowheads and white bar point out the bilayer thickness of 4 nm). **C**, a pear-tube diblock liposome. **D**, one block liposome encapsulated within another one (also seen in **E**, top arrow). **E**, a group of block liposomes. The block liposomes shown in **A-E** are comprised of liquid-phase lipid nanotube segments capped by spherical vesicles with diameters of a few hundred nm. The nanotubes (white arrows) are 10-50 nm in diameter and >1 μm in length. **F**, schematic depictions of the MVLBG2/DOPC tri- and diblock liposomes. **a** and **b** show molecular-scale illustrations, based on the hypothesized mechanism of BL formation (Zidovska *et al.*, 2009a), manifesting the symmetry breaking between outer and inner monolayer. In **A-E**, image contrast/brightness was altered in selected rectangular areas. Reprinted in part from (Zidovska *et al.*, 2009a) with permission. Copyright 2008 American Chemical Society.

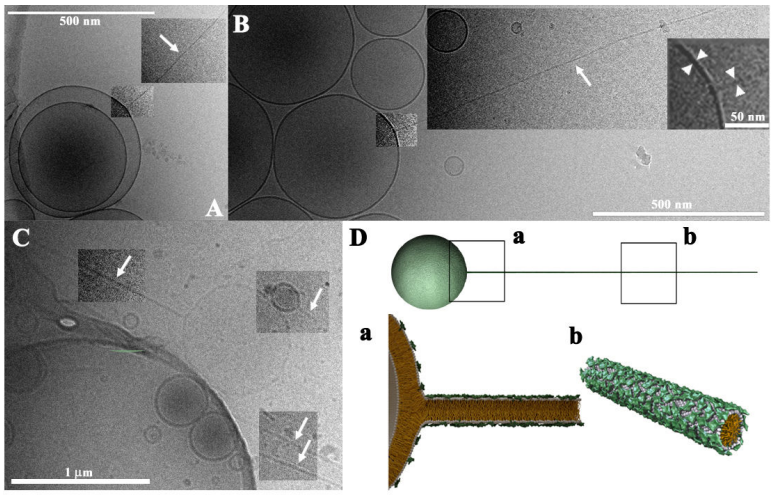

Figure 8. Cryo-TEM images of block liposomes containing liquid-phase lipid nanorods

A-D, diblock liposomes comprised of lipid nanorods (white arrows) connected to spherical vesicles. Lipid nanorods are stiff cylindrical micelles with an aspect ratio ≈1000. Their diameter equals the thickness of a lipid bilayer (≈4 nm) and their length can reach up to several μm with a persistence length of the order of mm. **C** (an inset of **B**) allows comparison of the thickness of the nanorod and the bilayer of the spherical vesicle: white arrow heads point out a thickness of ≈4 nm. Of note, free nanorods were not observed in any of the 426 cryo-TEM images analyzed. **E**, schematic of a MVLBG2/DOPC sphere-rod diblock liposome. Insets **a** and **b** show molecular-scale schematics based on the hypothesized mechanism of BL formation (Zidovska *et al.*, 2009a). Note the high concentration of MVLBG2 in the nanorod segment. In **A–D,** image contrast/brightness was altered in selected rectangular areas (Zidovska *et al.*, 2009a). Reprinted in part from (Zidovska *et al.*, 2009a) with permission. Copyright 2008 American Chemical Society.

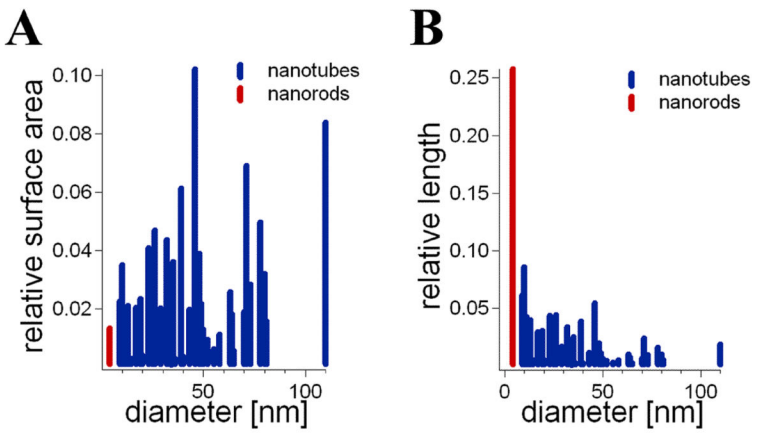

Figure 9. Statistical analysis of the nanotube and nanorod populations

A, diameter histogram weighted by the surface area, indicating the relative amount of lipid in the nanorod and nanotube state. **B**, diameter histogram weighted by the length of the structure, highlighting the striking length of nanorods compared to nanotubes. Reprinted in part from (Zidovska *et al.*, 2009a) with permission. Copyright 2008 American Chemical Society.

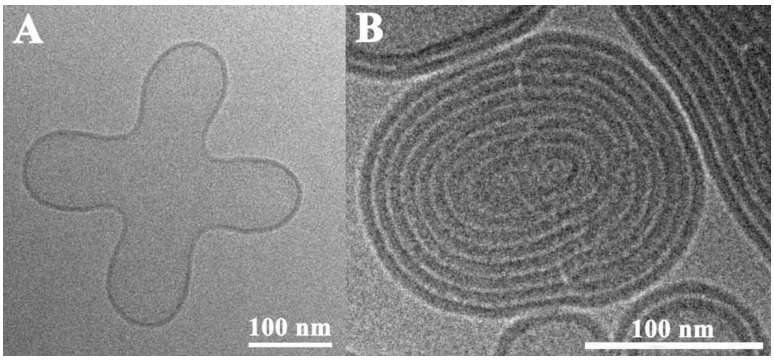

Figure 10. Cryo-TEM images providing insights into block liposome formation

A, an example of four simultaneous nanotube formation processes. The lack of a preferred orientation of the protrusions proves that they were not generated by flow effects. **B**, block liposomes transform into multilamellar spherical vesicles when the electrostatic forces are screened by presence of salt (250 mM NaCl, Debye length ≈0.6 nm). Reprinted in part from (Zidovska *et al.*, 2009a) with permission. Copyright 2008 American Chemical Society.

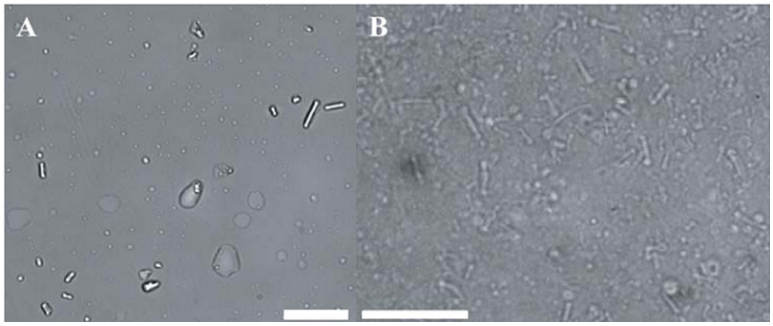

Figure 11. Dehydration and rehydration of BLs

A, DIC micrograph of dehydrated block liposomes. Note that the spherical caps at the end of the cylindrical core are collapsed. **B**, DIC micrograph of the sample shown in (**A**) after rehydration. The block liposomes have regained their original shape. Scale bars, 10 μm.